HEATING OF GLASS BY ELECTROMAGNETIC INDUCTION

Elías Carrillo[1], Miguel Angel Barrón[1]*, Jesús González[2], Antonio de Ita[1]
[1]Departamento de Materiales, [2]Departamento de Sistemas
Universidad Autónoma Metropolitana Azcapotzalco
Apdo. Postal 16-137, C.P. 02011, México, D.F., México
*E-mail bmma@correo.azc.uam.mx

ABSTRACT
An assembly for heating of molten glass using electromagnetic induction at low frequency is proposed, which consists of a central metallic column acting as a magnetic flux suppresser surrounded by a shell of molten glass contained in a cylindrical vessel. Molybdenum and liquid tin, the latter contained by a refractory barrier, are considered as magnetic shields. A thermal analysis of the process is included by coupling the energy equation with Maxwell equations, and considering molten glass as a rigid body. The model considers a rotary magnetic strength parallel to the angular coordinate as excitation source. A two-pole configuration has been selected for inductor coils whose objective is the enhancement of the electromagnetic coupling and the improvement of the power factor. In accordance with the numerical simulations results, the proposed arrangement shows feasibility for glass induction heating at 60 Hz.

Keywords: induction heating, magnetic shield, molten glass.

1. INTRODUCTION

Induction heating in molten glass involves some drawbacks due to its poor electrical conductivity. The occurrence of eddy current in molten glass is achieved mainly by means of high frequency with the concomitant inconvenient of frequency converter cost. On the other hand, to overcome the lack of electromagnetic coupling when using low frequencies, the process is carried out by means of susceptors[1], being those materials that are readily heated by induction and indirectly give off heat to electrically nonconductive materials through radiation or conduction heat transfer processes. However, the use of susceptors diminishes the appeal that represents high rates of heating and the efficiency associated to standard induction heating. The problem with induction heating in ionic liquids such as molten glass, is due to their incapacity to set proper decay in the distribution of the induced magnetic fields, in accordance to Lenz's law. Induction heating is usually accomplished using stationary magnetic fields. On the other hand, there are reports[2],[3] that traveling fields produced by poly-phased configuration in inductors lower skin depth δ, known as the boundary layer, beyond magnetic field vanishes as a result of the induction process.
As is well known, flux concentrators and magnetic shields are current practice for improving patterns of heating [4]. Flux concentrators, being made of high magnetic permeability materials, are commonly inserted within a circular coil for collapsing magnetic fields at its axis and to provide a higher magnetic flux density nearby coil surface. In the same manner, undesirable external and end fields from an excitation coil are cancelled by placement of a highly conductive non-ferrous metal known as magnetic shield. Above Curie temperature, the relative magnetic permeability in flux concentrators drops to unity. Unlike flux concentrators, the electrical conductivity in shields is not lost at high temperatures. With all above remarks, in this work it will be explored the field suppressing capabilities of two metals that do not react with molten glass. First, a cylindrical rod made of molybdenum is located at the center of the vessel, making direct contact with a molten glass shell. Secondly, liquid tin is contained by a physical barrier made of dense refractory placed in between, in order to maintain cylindrical shape for the tin bath. The whole assembly is supposedly excited with an external axial coil having a configuration of an induction motor. The aim is to establish theoretical conditions for the occurrence of an effective induction heating of molten glass at 60 Hz.

2. BASIS OF INDUCTION HEATING

The main reason for studying eddy current is their related effects, e.g. electromagnetic body forces and ohmic heating; the latter comprises the foundations for induction heating. The expression that describes the behavior of eddy current in a conductive medium, which is obtained by combining the Maxwell electromagnetic equations[5] is as follows:

$$\nabla^2 \mathbf{H} + \sigma\mu\nabla \times \left(\mathbf{v} \times \mathbf{H}\right) = \sigma \cdot \mu \frac{\partial \mathbf{H}}{\partial t} \tag{1}$$

Eq. (1) is expressed in terms of the magnetic strength vector **H** [$A \cdot m^{-1}$], whereas σ is the electric conductivity [$S \cdot m^{-1}$] and μ is the magnetic permeability [$V\ s\ A^{-1} m^{-1}$]. Here, the advective contribution is due to conductive

fluid velocity **v** [ms^{-1}]. The Hartman number, Ha, is a dimensionless parameter used for assessment of the aforementioned contribution:

$$Ha = \mu \cdot HR\sqrt{\frac{\sigma}{\eta}} \tag{2}$$

R is the characteristic length for the scaling [m], and η is the dynamic viscosity [$kgm^{-1}s^{-1}$]. The melting processes in metals involve temperatures above Curie temperature, so the magnetic permeability is that of vacuum space μ_0. The squared of the Hartman number $(Ha)^2$ embodies the ratio of electromagnetic forces to shear forces[6]. Hartman numbers in metals industry are much more greater than unit (Ha >>1), and are related to fluid movement that stirs hot bath in induction furnaces, thus enhancing both solid particle dissolution and homogenization. As a comparison, electro-magnetically driven flows in liquid metals, as in most laboratory experiments or industrial processes, keep velocity to a level of around 0.001 ms^{-1} to 1 ms^{-1}[6]. Generally speaking, $\sigma_{metals} \approx 10^6 \sigma_{glass}$ and with regard viscosities, $\eta_{metals} \approx 5X10^{-4} \eta_{glass}$. The root-squared ratio for each case would be:

$$\sqrt{\frac{\sigma}{\eta}}\Bigg|_{metals} \cong \sqrt{\left(\frac{\sigma}{\eta}\right)\frac{10^6}{5x10^{-4}}}\Bigg|_{glass} \tag{3}$$

Substituting Eq. (3) in Eq. (2) with the same characteristic length scale indicates that the magnetic strength in the corresponding molten glass processes should be about $\sqrt{2X10^5}$ higher than that occurring in molten metal operations. Therefore, Hartman numbers in glass systems would hardly be greater than unit, so the induced Lorentz force will not overcome the viscous forces to set motion in molten glass. Moreover, the advection term in Eq.(1) is affected by the free space magnetic permeability μ_0, which is such a small number; hence the velocity should be neglected. Therefore, by eliminating the second left-hand term in Eq.(1), the eddy current equations for a rigid body are obtained and might be suitable for molten glass, given that it is a very viscous fluid.

According to Faraday's law, when a time-varying magnetic flux passing through a given conductor, commonly known as work-piece, a voltage drop V_{work} arises in the excitation coil:

$$V_{work} = -N_c \frac{d\Phi}{dt} \tag{4}$$

where N_c is the number of coil turns in the working coil, and Φ is the integrated total magnetic flux inside the work-piece, which is of complex nature:

$$\Phi = \mu \int \left(\mathrm{Re}H + i\,\mathrm{Im}H\right) \cdot dA \tag{5}$$

In the above equation *A* is the area which is orthogonal to the magnetic flux. In the frequency domain, time dependence ($\partial/\partial t$) of Eq. (4) is substituted by $i\omega$, being ω [s^{-1}] the angular frequency of the excitation source and *i* equal to$\sqrt{-1}$. Thus, substituting Eq. (5) into Eq. (4):

$$V_{work} = \omega\mu_0 N_c \left(\int \mathrm{Im}H \cdot dA - i\int \mathrm{Re}H \cdot dA\right) \tag{6}$$

Since the active power comes from the real part of the field variables, it can be seen from Eq. (6) that the magnitude of the imaginary part of the induced field plays a very important role in the process of induction.

3. EFFECT OF COIL CONFIGURATION ON THE SHIELDING PROCESS

Most of the induction machines are shaped as a cylinder, in which there are two kinds of external configuration for the excitation coils, namely:

1.- The solenoid type as in coreless induction furnaces, where the excitation magnetic strength H_z is stationary and parallel to the axis of the cylinder.

2.- The induction motor winding, with its excitation angular magnetic strength H_φ. Here the traveling behavior is featured by a wave propagation vector **k**, whose components are the wave numbers. The number of pair of poles *p,* is considered equal to the wave number[7] .

3.1 Electromagnetic diffusion equation in cylindrical coordinates

In order to see how either φ or z magnetic strength are distributed inside the conductor, Eq. (1) is solved for the corresponding components. The field is expected to decay toward axis. To avoid dealing with end effects, an infinitely long conducting cylinder is assumed. Besides,

$$H_{\varphi}(z) = cte, \qquad H_z(\varphi) = cte \tag{7}$$

The component H_r has been neglected by the sake of simplicity. With those assumptions, the following expression is obtained from Eq. (1):

$$\frac{d^2H_w}{dr^2} + \frac{1}{r}\frac{dH_w}{dr} - \frac{H_w}{r^2} + \frac{1}{r^2}\frac{d^2H_w}{d\varphi^2} = \sigma\mu\frac{dH_w}{dt} \tag{8}$$

which is a generic electromagnetic diffusion equation applicable to either H_φ or H_Z, depending of what label subscript *w* had been taken .Using separation of variables, solutions for Eq.(8) are expressed as follows:

$$\left.\begin{aligned} H_w(r,\varphi,z,t) \equiv \left(\operatorname{Re} H_w(r) + i\operatorname{Im} H_w(r)\right)\exp i\left(\omega t - p\varphi\right) \end{aligned}\right\} \quad p = 0, \ \text{if} \ \ w = \mathrm{z} \tag{9}$$

Substituting Eq. (9) in Eq. (8), a system of coupled equations is obtained:

$$\left.\begin{aligned} \frac{d^2 \operatorname{Re} H_w}{dr^2} + \frac{1}{r}\frac{d \operatorname{Re} H_w}{dr} - \left(\frac{1+p^2}{r^2}\right)\operatorname{Re} H_w + \underbrace{\sigma\mu\omega}_{R_\omega}\operatorname{Im} H_w = 0 \\ \frac{d^2 \operatorname{Im} H_w}{dr^2} + \frac{1}{r}\frac{d \operatorname{Im} H_w}{dr} - \left(\frac{1+p^2}{r^2}\right)\operatorname{Im} H_w - \overbrace{\sigma\mu\omega}^{R_\omega}\operatorname{Re} H_w = 0 \end{aligned}\right\} \quad p = 0, \ \text{if} \ \ w = \mathrm{z} \tag{10a,10b}$$

With regard to complex plane, real zero is equalized to the right-hand term of Eq. (10a), whilst right-hand term in Eq. (10b) corresponds to zero of the imaginary ordinates. By applying dimensional analysis via differential equations to Eq. (10a) or Eq. (10b), a dimensionless number R_ω arises, namely the shielding parameter, which is related to the ability of a conducting medium to exclude high-frequency magnetic fields from its core:

$$R_\omega = \sigma\mu\omega \cdot R^2 \tag{11}$$

and features the ratio between the characteristic length scale of the conductor and the thickness of the electromagnetic skin depth δ = $\sqrt{(2/\sigma\mu\omega)}$. Then,

$$R_\omega = 2\left(\frac{L}{\delta}\right)^2 \tag{12}$$

Practical shielding parameters ranges around 20[8]. Typically a soda-lime molten glass has an electric conductivity of 28 $S{\cdot}m^{-1}$ and its magnetic permeability belongs to that of the vacuum space. If it is to be contained in a heating device of the same size of a metal melting furnace, frequencies around 1 MHz are needed in order to match the above R_ω parameter. On the other hand, a heating device of 40 m radius is required for a frequency of 60 Hz .

The following normalizations for the primitive variables convert Eqs. (10a) and (10b) into a pair of dimensionless coupled equations. The dimensionless radius χ is defined as the ratio between outer radius *R* that surrounds work-piece to radius *r*:

$$\chi = \frac{r}{R} \tag{13}$$

R might be referred as the work-piece characteristic length. The electromagnetic variables are normalized to the absolute value of the real part of the surface magnetic strength:

$$\Sigma = \frac{\mathrm{Re}\, H_\varphi}{\left|\mathrm{Re}\, H_\varphi(r=R)\right|} \quad , \quad \Psi = \frac{\mathrm{Im}\, H_\varphi}{\left|\mathrm{Re}\, H_\varphi(r=R)\right|} \tag{14}$$

The electromagnetic properties of the material are gathered in the shielding number R_ω.In this way, a set of simultaneous ordinary equations for Eqs. (10a) and (10b) are built, and solved by the shooting Newton method [9] with the following labels:

$$y_1 = \frac{d\Sigma}{d\chi}, \qquad y_2 = \frac{d\Psi}{d\chi}, \qquad y_3 = \Psi, \qquad y_4 = \chi, \qquad y_5 = \Sigma, \tag{15}$$

Boundary values for the magnetic fields at the axis are fixed to cero to allow the cancellation of fields in that point. The value of y_4 at left boundary is assumed nearly cero, e.g. 10^{-8}, for avoiding singularities. The non-dimension real magnetic strength is set to unity. The error to converge the solution is less than 10^{-8}. Various values of R_ω for H_φ were tried seeking for the lowest possible, accomplishing a smooth decay, and comparing to H_φ distribution maintaining R_ω = 20. The minimum pair of poles (p=1) yielded the higher values of the imaginary part of the magnetic strength. In Figure 1, both distributions are shown assuming R_ω = 7.75 as the lowest shielding parameter where at least the imaginary part of the magnetic strength has the same value than the real part at the surface.

In spite of the imaginary magnetic strength H_φ at the surface is 2.4 times greater than its counterpart H_Z, the angular imaginary magnetic flux is 85.73 % the total axial flux, as it can be seen in Table 1. Nevertheless, in an excitation axial coil, either frequency or radius of the cylinder can be reduced while keeping constant electrical conductivity compared to an excitation circular coil with no detrimental of real active power.

Table 1. Dimensionless Electromagnetic Parameters

Shielding Parameter R_ω		Total Imaginary Magnetic Flux per length $\int \lvert \mathrm{Im}H_w \rvert \, dr$	Current per length $\frac{1}{2}\int \lvert J_w \rvert^2 r$	Imaginary Magnetic Strength at surface $\lvert \mathrm{Im}H_w \rvert$
w=z	20	0.12611	1.3807	0.4146
w=φ	7.75	0.11039	2.2345	0.9955

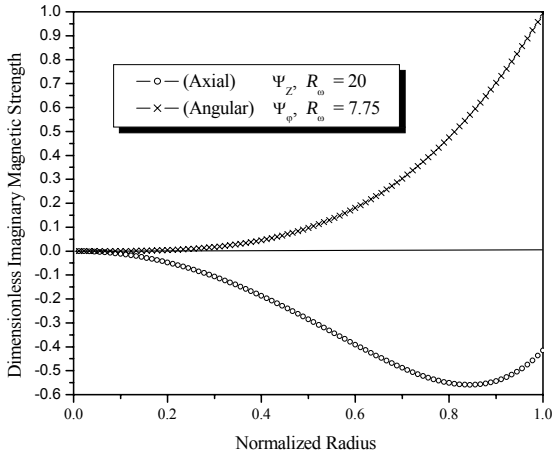

Figure 1. Imaginary magnetic strength decay for a cylinder excited by axial and angular excitation fields.

3.2 Ohmic heating

The assessment of the volumetric Joule dissipation P_w is carried out by integrating the real part of the mean (time-averaged) current density, according to the Poynting theorem [5]:

$$P_w = -\iiint_{Vol} \frac{\overline{J_w^2}}{\sigma} dr \cdot r d\varphi \cdot dz \tag{16}$$

For harmonic variables, the time averaged current density is obtained by means of this expression:

$$\overline{J_w^2} = \frac{1}{2}\mathrm{Re}\left(J_w \cdot J_w^*\right) = \frac{|J_w|^2}{2} \tag{17}$$

The superscript (*) on Eq. (17) represents the complex conjugate of J_w and the term inside brackets is the complex module of J_w. With previous knowledge of distributions of magnetic strength inside work piece, the current density **J** can be calculated by applying the Ampere's circuital law for low frequencies, the so called quasi-stationary approach[10]

$$\nabla \times \mathbf{H} = \left(J_r, \quad J_\varphi, \quad J_z\right) \tag{18}$$

Developing curl **H**, Eq. (18) in cylindrical coordinates for both φ and z current density component, and taking in account the remarks pointed on Eq. (7), these expressions are obtained:

$$J_\varphi = -\frac{d\left(\mathrm{Re}\, H_Z\right)}{dr} - i\frac{d\left(\mathrm{Im}\, H_Z\right)}{dr} \tag{19}$$

$$J_Z = \frac{\mathrm{Re}\, H_\varphi}{r} + \frac{d\left(\mathrm{Re}\, H_\varphi\right)}{dr} + i\left(\frac{\mathrm{Im}\, H_\varphi}{r} + \frac{d\left(\mathrm{Im}\, H_\varphi\right)}{dr}\right) \tag{20}$$

The scalar component of J_r has been neglected. Continuing with the non-dimensional analysis between the two coaxial winding treated above, the current density distribution is obtained by substituting Eqs. (13) and (14) in Eq. (19) and then in Eq. (17):

$$\left.\overline{J_\varphi^2}\right|_{\text{dimensionless}} = \frac{1}{2}\left(\left(-\frac{d\Sigma_Z}{d\chi}\right)^2 + \left(-\frac{d\Psi_Z}{d\chi}\right)^2\right) \tag{21}$$

for the dimensionless angular current density. In a similar fashion, by replacing Eqs. (13) and (14) in Eq. (20) with the form of Eq. (17), the dimensionless axial current density is obtained:

$$\left.\overline{J_Z^2}\right|_{\text{dimensionless}} = \frac{1}{2}\left(\left(\frac{d\Sigma_\varphi}{d\chi} + \frac{\Sigma_\varphi}{\chi}\right)^2 + \left(\frac{d\Psi_\varphi}{d\chi} + \frac{\Psi_\varphi}{\chi}\right)^2\right) \tag{22}$$

Both density currents are plotted in Figure 2. The third column of Table1 shows the electric current per length integrated from Figure 2. It can be seen that the additional term in Eq. (22) related with Eq. (21) yileds more power for a given work-piece.

4. EFFECT OF INSERTION OF A METAL COLUMN IN THE SHIELDING PROCESS

Although the configuration of an excitation axial coil seems promising, the problem remains unsolved since at 60 Hz the shielding parameter with a value of 7.75 for molten glass implies a furnace radius of nearly 25 meters. Such size is still big for a practical purposes. Therefore, the pattern that is found in poor conductors at low shielding parameters is intended to be modified by using flux concentrators or shields in order to have the magnetic field at the axis cancelled in relatively small cylinder radii.

The dimension of the proposed assembly for the composite work-piece is shown in Table 2. The magnetic shield is occupying one third of the total radius for a molybdenum assembly and takes 30.21% of the total radius for the tin assembly.

4.1 Continuity of magnetic and temperature fields

The tangential component of the magnetic strength field has the same value at interfaces of different materials, allowing its continuity. This is a consequence of the well-known rule in electromagnetism[5] for boundary conditions:

$$\mathbf{n}_{inner} \times \mathbf{H}_{inner} + \mathbf{n}_{outer} \times \mathbf{H}_{outer} = (0,0,0) \tag{23}$$

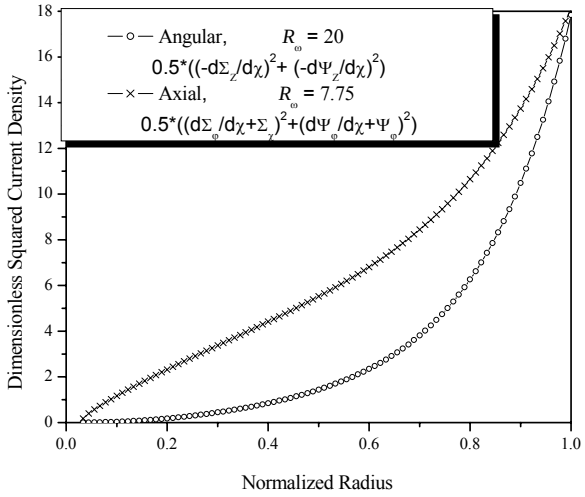

Figure 2. Module of density current for a cylinder excited by axial and angular excitation fields.

Table 2. Arrangement of the work-piece.

Cylindrical assembly	Shielding Column radius	AZS Barrier Thickness	Molten Glass thickness	Tri-phase kW per length
Molybdenum	0.25 [m]	----------	0.5 [m]	64
Tin	0.4 [m]	0.13 [m]	0.795 [m]	253.5

where **n** is the unitary vector normal to the limiting surface. Due to the assumed stiffness of molten glass and the suppressed magnetic field in the tin bath, there will not be electromagnetic driven flows, so the heat transfer process is thoroughly carried out by conduction through shield, barrier and molten glass. Because the ohmic heating is mainly released along radius, the thermal analysis will be undertaken in one-dimension and in steady state. Thus, the applicable form of the energy equation is:

$$\nabla^2 T = \frac{|J_Z|^2}{2\lambda\sigma} \tag{24}$$

Where T is temperature [°C], λ is the thermal conductivity [$Wm^{-1}K^{-1}$] which is assumed independent of temperature. It represents the Joule loss per unit volume in the bulk. Since the axial coil configuration seems to have better performance, the subscript *w* is equalized to z and the further analysis will be focused on it. By considering the axial density current according to Eq. (17) and Eq. (20) in Eq. (24), then:

$$\frac{d^2T(r)}{dr^2} = -\frac{1}{r}\frac{dT(r)}{dr} + \frac{1}{2\lambda\sigma}\left(\left(\frac{\mathrm{Re}\,H_\varphi(r)}{r} + \frac{dH_\varphi(r)}{dr}\right)^2 + \left(\frac{\mathrm{Im}\,H_\varphi(r)}{r} + \frac{dH_\varphi(r)}{dr}\right)^2\right) \tag{25}$$

Given that the source term in Eq. (25) is expressed in terms of the angular magnetic strength H_φ, it can be coupled with Eq. (10a) and Eq. (10b) when fixing subscript *w*=φ. This system yields the governing equations of the process. This system of ordinary differential equations (ODE) can be solved using the Newton shooting method, which was built taking the following designations:

$$y_1 = \frac{d\,\mathrm{Re}(H_\varphi)}{dr}, \quad y_2 = \frac{d\,\mathrm{Im}(H_\varphi)}{dr}, \quad y_3 = \mathrm{Im}(H_\varphi), \quad y_4 = r, \quad y_5 = \mathrm{Re}\,H_\varphi, \quad y_6 = T, \quad y_7 = \frac{dT}{dr} \tag{26}$$

The first five equations of the above ODE system with their boundary conditions were set as above dimensionless case. Regarding boundary conditions for the last equation y_7, left boundary value was

guessed zero as initial shot, and right boundary was tried with several values until consistency with surface power density was obtained. Given that continuity of magnetic strength through internal boundaries is allowed as is given by Eq. (23), the numeric code was included with an instruction for changing values of electric conductivity at the time the computation crosses the interface. The same procedure was implemented for the continuity in thermal conductivities through different regions. Due to the significant difference in physical properties for each region (see Table 3), the relaxation for error in convergence had to be less than 0.005.

Table 3. Physical Properties

Conductivities	Molybdenum (1350°C)	Tin (710°C)	AZS (750°C)	Molten Glass
Thermal (λ)	86	33.5	3.6	11
Electric (σ)	2.5 (10^6)	1.633 (10^6)	0.1428	σ(T) as in Eq.(27)

As is well known, several properties of the involved materials described in the coupling equations depend on temperature, however in this work only the functionality of the electric conductivity of molten glass was considered:

$$\sigma_{glass} = 2500 \exp\left(\frac{-7599}{T + 273.15} \right) \tag{27}$$

The above electric conductivity expression is that belonging to a glass whose composition is as follows: 72.3 weight percent SiO_2, 0.4% Al_2O_3, 8.5 % CaO, 14.3 % Na_2O, 3.8 % MgO, and was obtained by adopting the Rasch and Hinrichsen equation.[11].The chosen refractory is supposedly made of dense electro-cast AZS with 32.5 % ZrO_2 , which is resistant to corrosion by molten glass[12].

5. NUMERICAL SIMULATIONS

The numeric simulations were based on tentative conditions for improving the overall power factor keeping the minimum radius in the induction device. The contribution of the reflected resistance from the composed work-piece is proportional to the first term inside brackets in Eq. (6) whilst the reflected inductive reactance is function of the second term. The integrated imaginary magnetic flux is fixed in 1.5 times the integrated real magnetic flux. Those values were achieved having a total radius of 0.75 m and 1.32 m for the molybdenum and tin assemblies, respectively. A rotating magnetic strength H_0 featured by number of poles p = 1 at 60 Hz is imposed in the cylinder surface with values of 150 A m^{-1} and 175 Am^{-1} for corresponding cases. The magnetic distributions as a solution of Eq. (26) are plotted in Figures 3 and 4. The current density, calculated according to Eq. (20), is plotted in Figures 5 and 6, and shows a decay in the metal zone, as expected. Then, there is a sudden increase of the current density in molten glass region where the magnetic flux is concentrated. This causes the ohmic heating be released in this region. An isotherm is produced in the metal region as a result of the shielding process, as is shown in Figures 3 and 4. Whereas the electric conductivity in metals decreases as temperatures increases, in molten glass occurs in another way. Temperature of 1350°C is relatively high but is typical for molybdenum used in molten glass operations. However, the electric conductivity of Mo (see Table 3) allows lower molten glass temperatures than those in the tin assembly (see Figure 4). There, molten glass is hotter for better electric conduction in that zone, in order to compensate the lower tin electric conductivity. The tin bath temperature was set to 710°C seeking higher conductivity for shielding purposes.

The kernel of integral in Eq. (16) for w=z is plotted in Figures 7 and 8. The curves with the development shown in Eq. (20) follow closely the gradient temperature. The total surface power density is obtained by integrating such kernel, using ⅓Simpson rule. Also, the power density is obtained by applying the Fourier rate law, which is -λ dT/dr everywhere[13]. This energy front allowed temperatures which were coherent with conductivities. At the surface, the heat flux area is $2\pi Rz$, and z is the unitary length. At the cylinder surface both procedures yield 255 kW for tin and 63 kW for molybdenum, which match the rated power shown in Table 2.

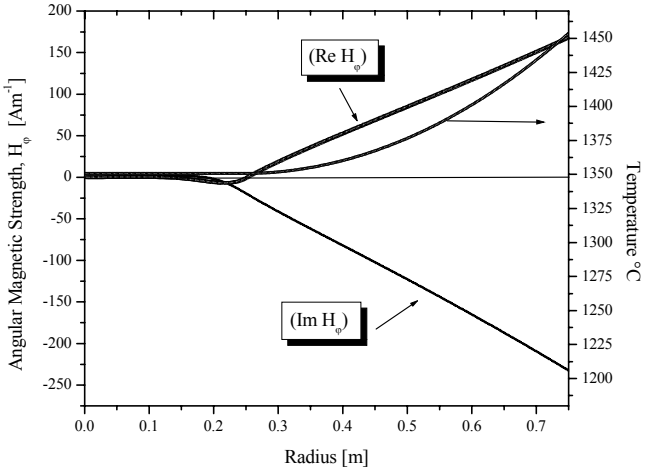

.

Figure 3. Radial distribution of magnetic strength and temperature in a composed cylinder using a molybdenum insertion.

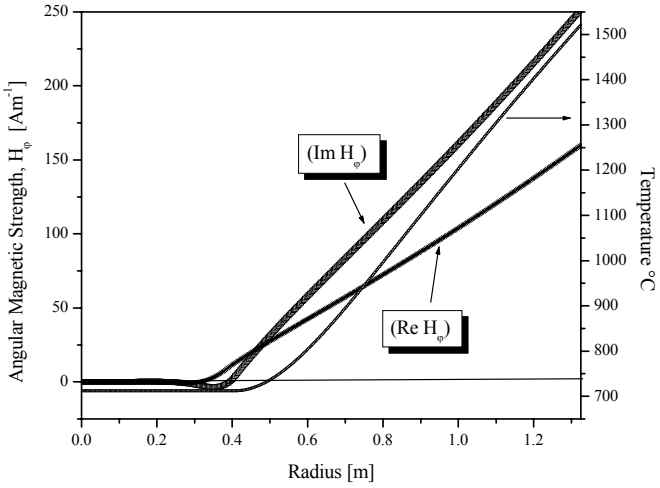

Figure 4. Radial distribution of magnetic strength and temperature in a composed cylinder using a tin insertion.

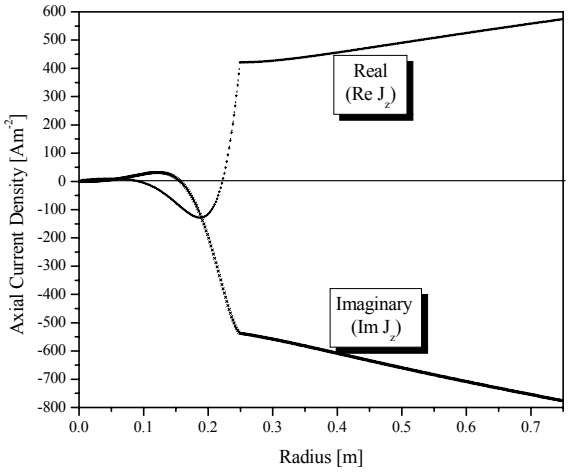

Figure 5. Current density radial distribution in a composed cylinder using a molybdenum insertion.

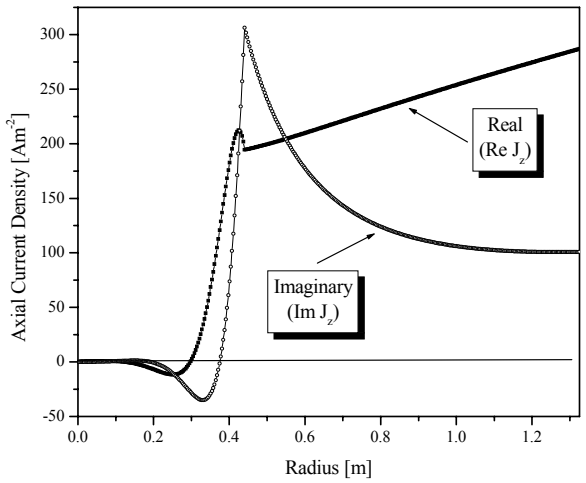

Figure 6. Current density radial distribution in a composed cylinder using a tin insertion.

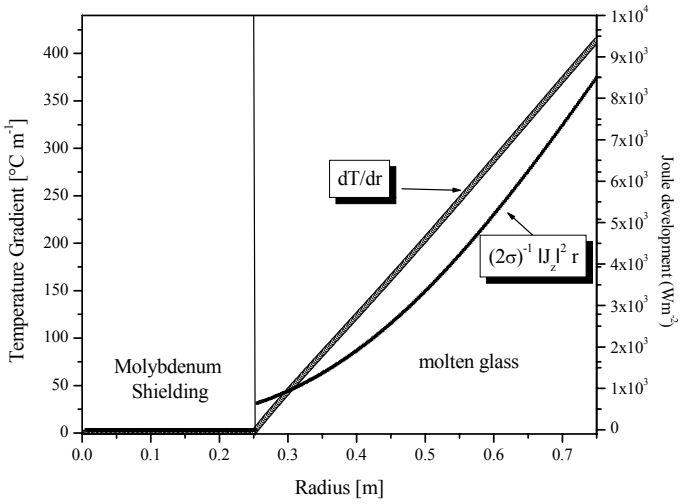

Figure 7. Joule development and temperature gradient in a composed cylinder using a molybdenum insertion.

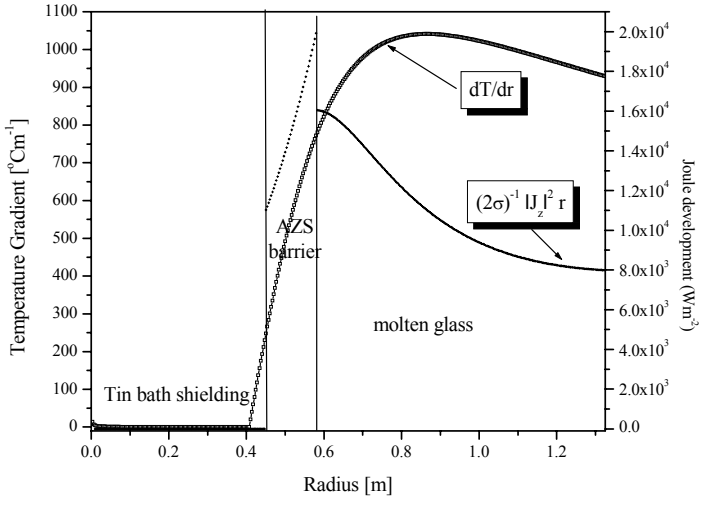

Figure 8. Joule development and temperature gradient in a composed cylinder using a tin insertion.

6. CONCLUDING REMARKS

In the search of an alternative technology for heating of molten glass, an electromagnetic induction method which employs mains frequency was proposed. Instead of considering huge coils and work-pieces according to skin depth formula, magnetic shielding was considered in order to reduce the furnace size. Besides, a theoretical arrangement was developed using a traveling magnetic field as excitation source. This arrangement shows feasibility of molten glass heating by electromagnetic induction for a heating device with radius as small as 0.75 m. It is expected that this theoretical application be promising for a future construction of an industrial-scale furnace.

ACKNOWLEDMENTS

This work was supported by CONACYT (Mexico). Grant No. 174697. Thanks to CONACYT for a Doctoral Fellowship.

REFERENCES

1. Ducharme, R., Scarfe, F., Kapadaia, P. and Dowden, J. The Induction heating in glass. *Journal of Physics-D*, 24 (1991) 658-663.
2. Szekely, J., Chang, C. Turbulent electromagnetically driven flow in metals processing. Part 1: Formulation. *Ironm.& Steelm.*, 3 (1997)190-195.
3. Hughes, W.F., and Young, F.J. *The Electrodynamics of fluids.* John Wiley & Sons, 1966, USA, pp. 611-613.
4. Zinn, S., Semiatin, L. *Elements of induction heating: design, control, and applications*. Electric Power Research Institute, 1988, pp. 241-252.
5. Krawczyk, A., and Tegopoulos, J.A. *Numerical modeling of eddy current.* Clarendon Press, Oxford, 1993, pp. 5-8.
6. Davidson, P.A. *An introduction to magnetohydrodynamics*. Cambridge University Press, 2001, pp. 96-97.
7. Yannopoulos, P.P., and Tegopoulos, J.A. *Three dimensional eddy current distribution in cylinders due to rotating magnetic fields*. IEEE Trans. on Magnetics, MAG-23 (1987) pp. 3056-3058.
8. Zhao, C., and Fautrelle, Y. *Turbulent fluid flows in channel induction furnaces*. The Minerals, Metals & Materials Society, 1991, USA, pp. 151-157.
9. Constantinides, A. *Applied Numerical methods with personal computers.* McGraw-Hill, 1987, USA, pp. 418-439.
10. Steele, C.W. *Numerical computation of electric and magnetic fields*. Chapman & Hall , 1997, pp. 5.
11. Stanek, J. *Electric melting of glass*. Elsevier, 1977, pp. 50-54.
12. Trier, W. *Glass furnaces: design, operation and construction*. Table, 1981, pp. 77.
13. Davies, J., and Simpson, P. *Induction heating handbook*. McGraw-Hill Company, 1979, USA, pp. 359.